Oil-Immersion Stable Superamphiphobic Coatings for Long-term Super Liquid-Repellency

Xuan Jiaoa, Meiting Lia, Xinquan Yua, William S. Y. Wongb,*, and Youfa Zhanga,*

Chem. Eng. J. **2021**, 420, 127606. DOI: https://doi.org/10.1016/j.cej.2020.127606

Oil-Immersion Stable Superamphiphobic Coatings for Long-term Super Liquid-Repellency

Xuan Jiao[a], Meiting Li[a], Xinquan Yu[a], William S. Y. Wong[b,*], and Youfa Zhang[a,*]

a Jiangsu Key Laboratory of Advanced Metallic Materials, School of Materials Science and Engineering, Southeast University, Southeast Road 2nd, Nanjing 211189, P. R. China.

b Max Planck Institute for Polymer Research, Ackermannweg 10, D-55128 Mainz, Germany.

E-mail: wong@mpip-mainz.mpg.de, yfzhang@seu.edu.cn.

Chem. Eng. J. **2021**, 420, 127606. DOI: https://doi.org/10.1016/j.cej.2020.127606

Abstract: Superamphiphobic coatings have attracted tremendous interest from both academia and industry owing to their potential for self-cleaning and anti-fouling. However, many state-of-the-art superamphiphobic coatings are unable to preserve their super-repellent properties after prolonged liquid immersion. Thus, practical applications have so far been drastically limited. Herein, we highlight the immersion-stable performance of a nanostructurally-densified superamphiphobic coating possessing super liquid repellency to water and various low-surface-tension liquids. They exhibit excellent superoleophobic properties and functional stability even after prolonged immersion in mixed synthetic and vegetable oils. This immersion-stable superamphiphobic coating was also tested on household kitchen appliances under real-world conditions. Particularly inaccessible components such as the impeller and grease traps of range hoods were coated. Impellers demonstrate an improvement of up to 65% contamination-resistance while grease traps remained largely dry after collected oils were disposed. These findings highlight the potential of using nanostructurally-densified superampiphobic coatings as anti-fouling surfaces in the kitchen environment, with potential applications in petroleum extraction and oil transportation.

Keywords: Superamphiphobic, Oil-immersion, Long-term, Stability, Range hood

1. Introduction

Inspired by superhydrophobic plants such as the lotus (Nelumbo) [1], superamphiphobic surfaces with high static contact angles (≥ 150°) and sliding angles (≤ 10°) for both water and oil have received a lot of attention from academia and industry [2-7]. To achieve these peculiar surfaces, an appropriate combination of surface morphology and low surface energy is needed [8-13]. The low surface adhesion towards a wide range of liquids, including water, low-surface-tension oils, and organic solvents, allows for the ease of their removal without leaving any residue. Due to these multifunctional properties, they exhibit great potential for application in antifouling materials [14], self-cleaning coatings [15], chemical shielding [16] and oil transportation [17,18].

The use of superamphiphobic coatings for oily kitchen environments is particularly promising as anti-fouling coatings on grease traps, kitchen ventilation impellers, and kitchen exhausts. However, the adhesion and hardness of state-of-the-art coatings remain too fragile to be directly cleaned by scrubbing. Therefore, we propose the use of superamphiphobic coatings in difficult-to-reach components in appliances which are inherently shielded from contact (*i.e.* impeller and grease trap). During prolonged operation, most superamphiphobic coatings will experience immersion under different liquids (*i.e.* mixed oils). Subsequently, they are known to lose their super liquid repellency [19-23]. This is accompanied by shedding of the functional coating and subsequent penetration by oil drops. So far, long-term resistance to oil immersion is still fairly difficult to achieve (see Table S1). In other instances, researchers studied

the tunability of network fluoroalkyl densification on nanoparticles for super liquid-repellency but did not investigate prolonged oil-immersion [27]. Here, we propose to overcome these drawbacks by optimal surface functionalization and densified nano-structuring.

In previous literature, different kinds of superamphiphobic surfaces were prepared using spray-deposition to form hierarchical structures. These legacy surfaces tend to have large pore sizes [24], resulting in low breakthrough pressure. Inspired by such super-repellent surfaces, we first used high degrees of surface-fluorination *via* the means of cross-linked FDTS, which matches the lowest possible solid surface energy [25,26]. Thereafter, we improved upon the state-of-the-art, by the use of a highly compact nanoparticle coating, designed to have nano-scale pore sizes in order to enhance breakthrough pressure, thus resistance to prolonged oil-immersion.

Previously, Hsieh et al. have fabricated a stable superoleophobic surface using a hierarchical silica sphere stacking layer, which maintains its water and ethylene glycol repellency after immersion for at least three days [19]. With improvements to scalability, Wu et al. have prepared a series of superamphiphobic coatings based on hierarchical FOTS-SiO_2 powders, which displayed excellent super-repellency even after soaking in crude oil for ten days [20]. In other works, complicated synthesis methods and limited oil immersion resistance continue to hamper real-world applications [31-34]. To date, superamphiphobic coatings with abrasion resistance have been reported for various applications [28,29,30]. For instance, some are composed of fluorinated multi-walled carbon nanotubes that have been applied in anti-corrosion and self-cleaning [28]. However, these coatings are devoted to demonstrating enhanced mechanical robustness. Notably, abrasion resistance is not equivalent to oil-immersion resistance due to different breakdown mechanisms. Therefore, the focus of this work, on tuning liquid-repellency and long-term immersion performance remains rarely investigated.

Herein, we propose a simple methodology for fabricating immersion-stable superamphiphobic coatings. This is achieved first by spraying a primer resin coat and thereafter impregnating the resin layer with functionalized nanoparticles. The coatings exhibit high static contact angles and low sliding angles for a variety of low-surface-tension liquids. These coatings have the following advantages: (1) The coatings were facilely prepared by spray-deposition using pre-modified SiO_2 nanoparticles having high degrees of fluoro-densification; (2) The coatings exhibit stable superamphiphobicity toward mixed synthetic and vegetable oils under prolonged immersion with heating (up to 50 days at 80 °C). Coatings easily last beyond 60 days of immersion under ambient conditions.

2. Experimental section

2.1. Materials

Fluoroethylene vinyl ether (FEVE) resin, acrylic acid (AA) resin, polyurethane

(PU) resin, n-butyl acetate and curing agent (for fluorocarbon resins) were provided by Nanjing WanQing Chemical GlassWare & Instrument Co., Ltd. 1H,1H,2H,2H-perfluoro-decyltrichlorosilane (FDTS) and 1H,1H,2H,2H-perfluorodecyl-trichlorosilane was purchased from Aladdin (Shanghai) reagent Co., Ltd. Silica sol was purchased from Nanjing Super-roll New Material Technology Co., Ltd. Silica nanoparticles with a size of 10-20 nm, absolute ethanol (EtOH), ammonium hydroxide ($NH_3 \cdot H_2O$, 28 wt%), tetraethoxysilane (TEOS) were purchased from Sinopharm Chemical Reagent Co., Ltd. FEVE has been selected as a key component of the primer due to 1) Excellent adhesion to the substrate and 2) Low surface energy. The impellers and grease traps were provided by Hisense (Guangdong) Kitchen & Bath System Co., Ltd and BSH Electric Appliance (Jiangsu) Co., Ltd, respectively.

2.2. Preparation of the FEVE/AA composite primer

The primer composed of mixed resins was acquired by the dissolution of FEVE, AA, silica nanoparticles and curing agent in n-butyl acetate. The mass ratio of n-butyl acetate, FEVE, AA, nanoparticles and curing agents is 19.5:3:3:0.3:3. Firstly, FEVE and AA were dispersed in n-butyl acetate and stirred for 2-4 h. Silica nanoparticles were then added into the biphasic mixtures. Subsequently, curing agents were added to the mixtures, and continuously stirred for 10 min.

2.3. Preparation of the superamphiphobic nanoparticle suspension

1.2 g silica sol was diluted and alkalified in an alkaline solution containing 8 mL of deionized water and 4 mL of ammonium hydroxide. After ultrasonic dispersion for 10 min, the mixture was slowly added into 80 mL of EtOH with continuous stirring for 30 min. Subsequently, different amounts of FDTS was slowly added into the system (defined as wt % of the total mixture). The superamphiphobic nanoparticle suspension was obtained after the reaction was completed in 24 h.

2.4. Spray-coating of superamphiphobic coating

An airbrush (working distance = 10 cm, pressure = 60 bar, flowrate = 0.13 mL/s) was first used to coat the FEVE/AA composite primer onto the substrate (2.7 L/m^2). After semi-curing for several minutes at ambient temperature, the superamphiphobic nanoparticle suspension was sprayed onto the composite primer (8.5 L/m^2). Finally, this layered superamphiphobic coating was cured for 24 h at room temperature. The detailed process is presented in Fig. S1. Test samples (glass slides) were only coated on one side.

2.5. Surface Characterization

The morphology of samples was observed using a field-emission scanning electron microscopy (FESEM) and a transmission electron microscope (TEM), which were conducted using a Sirion instrument and a G2-20 instrument (FEI Corporation, Hillsboro, USA), respectively. The physical adsorption of N_2 at 77 K was performed via a fully automated surface area and porosity analyzer (Quantachrome, Florida, USA). Specific surface areas were determined by the Brunauer-Emmett-Teller (BET) method.

The static water contact angles (CAs) and sliding angles (SAs) were determined through an OCA 15Pro contact angle goniometer. Test samples were measured at five different positions and presented in mean ± standard deviation.

3 Results and discussions

3.1. Fabrication of superamphiphobic coatings

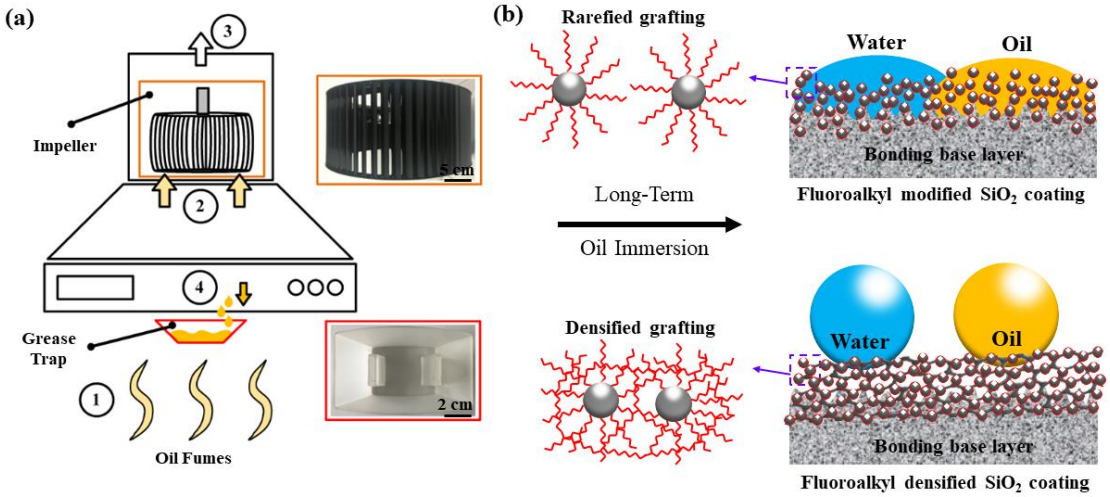

Fig. 1. A schematic representation of the hard-to-clean components of a range hood and the wetting properties of water and oils on superamphiphobic coatings. (a) The schematic of a typical range hood, highlighting components (red and orange boxes) that were coated by the as-prepared superamphiphobic coating. (b) (Top) The superamphiphobic coating embedded with fluoroalkyl modified SiO_2 (FM-SiO_2) nanoparticles was permeated by oil after immersion for a few days. (Bottom) The superamphiphobic coating embedded with fluoroalkyl densified SiO_2 (FD-SiO_2) nanoparticles displayed excellent oil immersion resistance for over 60 days.

Coatings were fabricated in a simple and highly efficient manner, as schematized in Fig. S1. The superamphiphobic coatings were prepared by the combination of a polymer composite primer and functional nanoparticles (See Experimental Section), and sprayed onto a variety of kitchenware components and other test substrates (Fig. S2, Video S1). Two differently- functionalized superamphiphobic coatings were used for comparative purposes, as schematized in Fig. 1. We know that 1H,1H,2H,2H-perfluoro-decyltrichlorosilane (FDTS, tri-functional) plays a crucial role in forming a network during functionalization. Self-condensation takes place spontaneously during the process. Covalent bonding takes place primarily between the hydroxyl groups on silica and the trichlorosilane groups (condensation), forming a primary functional layer on nanoparticles. With sufficient trichlorosilane, oligomers are able to form via stochastic self-condensation reactions occurring between the trichloro- functionalities of the silanes under ambient moisture (self-condensation). With excess trichlorosilane, oligomers further react to form a network. This represents the well-known network polymerization mechanism belonging to trichlorosilanes [35]. The proposed mechanism is presented in Fig. S3. Upon increasing the concentration of FDTS, the

degree of polymerization increases. Initially, a low concentration of FDTS (i.e. 0.21%) likely only induced the formation of a predominantly covalently-bonded fluoroalkyl modified layer on SiO_2 nanoparticles (FM-SiO_2). Using a high concentration of FDTS (*i.e.* 0.45 wt%) in the reaction results in denser (*ca.* 45 wt %) network-bonded fluoroalkyl layers on SiO_2 nanoparticles (FD-SiO_2), building on top of initial layers. Thus, superamphiphobic coatings embedded with FD-SiO_2 nanoparticles possess densified fluoroalkyl network packing at the sub-and-nanoscopic domains, potentially aiding in its long-term oil immersion stability. In contrast, the superamphiphobic coating embedded with the slightly less densely functionalized FM-SiO_2 nanoparticles (40 wt%) was found to be prone to higher oil adhesion and poorer oil immersion resistance (Fig. S4). This occurs despite achieving quasi-similar surface morphologies.

In the process of hydrolysis and fluoro-functionalization, FD-SiO_2 particles with hierarchical structures were obtained. The TEM images in Fig. 2a show that the functionalized nanoparticles were crosslinked and poly-condensed to some extent. On the contrary, untreated silica nanoparticles were comparatively discrete (Fig. S5). The surface morphology of the superamphiphobic coatings was characterized using FESEM. Fig. 2b and c show that the coatings were evenly distributed on the composite resin, highlighted by the presence of stochastic nanopores (11~184 nm). Supplementary SEM images with different magnifications are presented in Fig. S6. The dense micro- and nano-structured (hierarchical) surfaces are vital for the so-called Cassie-Baxter state which prevents wetting. In the SEM images of both FM-SiO_2 and FD-SiO_2, nanoparticles are assembled into aggregates which are anchored into the composite primer during coating, with a thickness of *ca.* 13 μm (Side views: Fig. S7). The resulting surfaces trap air within the hierarchical architectures, giving rise to excellent liquid repellency. In principle, there could still be minute differences in the morphology belonging to the two types of superamphiphobic coatings presented here. Nonetheless, the immersion resistance observed for the coating embedded with FD-SiO_2 was notably far superior to that embedded with FM-SiO_2 nanoparticles. We ascribe this improvement to both the improved degree of surface network functionalization, and the nanostructural packing of modified SiO_2 particles.

Specific surface area (SSA) analysis using the Brunauer–Emmett–Teller (BET) method is highlighted in Fig. 2d. Upon increasing the concentration of FDTS, the SSA of the fluorinated SiO_2 particles decreased from ~300 m^2/g (bulk silica) to 35 m^2/g (at a FDTS concentration of 0.45–0.60%). FM-SiO_2 nanoparticles had a SSA of 130 m^2/g compared to FD-SiO_2 nanoparticles' SSA of 30 m^2/g. Due to the network polymerization reaction, we believe that the crosslinking and multilayer stacking of fluoroalkyl chains formed a denser and thicker (cross-linked) network structure around the nanoparticles, resulting in the reduction of measured surface area. Notably, the change in SSA was only stabilized at relatively high reaction concentrations (*i.e.* 0.45

w/w %) of FDTS.

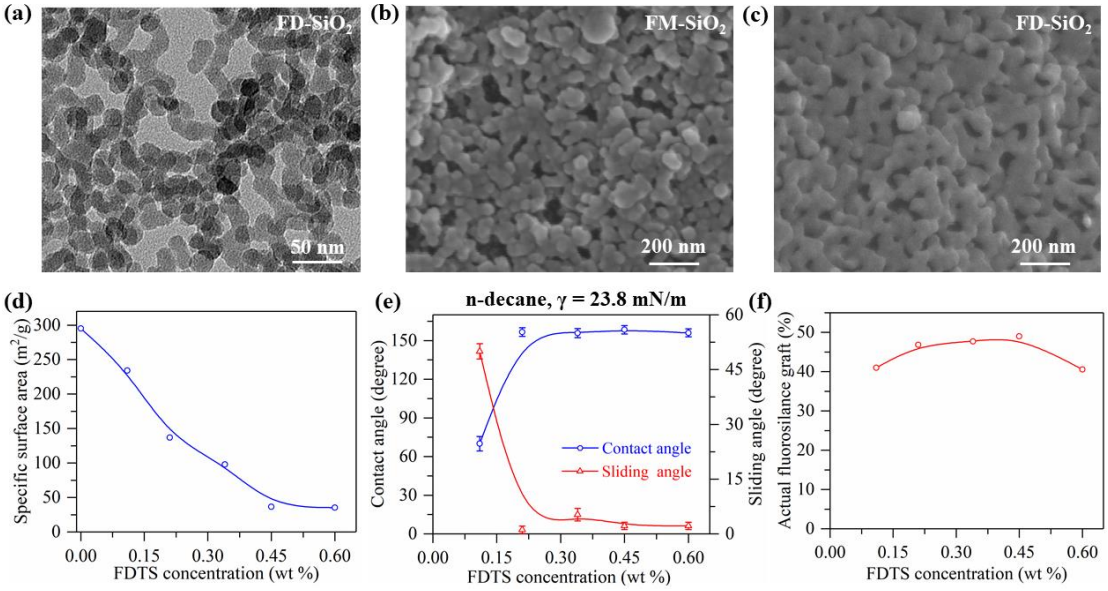

Fig. 2. Characterization of the network-functionalized silica nanoparticles and the wetting properties of the superamphiphobic coatings. (a) TEM image of the FD-SiO_2 nanoparticles. (b) SEM image of the superamphiphobic coating embedded with FM-SiO_2 nanoparticles. (c) SEM image of the superamphiphobic coating embedded with FD-SiO_2 nanoparticles. (d) The specific surface area analysis of fluoro-functionalized nanoparticles treated with various reaction concentrations of FDTS. SSA results describe the evolution of a denser and thicker functional network layer. (e) The variation of FDTS concentration and its influence on contact and sliding angles of n-decane on superamphiphobic coatings. (f) The effect of FDTS concentration on the actual fluorosilane grafted on nanoparticles (represented as a w/w ratio).

The wettability of the superamphiphobic coatings was assessed using contact angle goniometry with n-decane (γ = 23.8 mN/m). These tests revealed high static contact angles (> 150°) and low sliding angles (< 10°) upon achieving the surface grafting density of beyond 45 wt%. The equilibrium plateau observed for CA and SA in Fig. 2e demonstrates that coatings remain non-wettable towards the low-surface tension liquid, therefore achieving superamphiphobicity [36]. Despite showcasing similar repellency to n-decane, the density of grafted fluorosilanes is slightly dependent on the reaction concentration of FDTS. This analysis was supplemented by TG analysis, as shown in Fig. S8, which provides a direct measurement of grafted fluorosilane. The weight loss observed in the TG curves from 400 to 590 °C represents the weight percentage of grafted fluorosilane. The results in Fig. 2f indicate an optimal reaction composition for the network polymerization reaction. Grafting functionalization of SiO_2 nanoparticles at a FDTS reaction concentration of 0.45 wt% provides the maximum degree of densification. These have so-far been referred to as the fluoroalkyl densified SiO_2 (FD-SiO_2) nanoparticles. As for the particles treated at a comparatively

low FDTS reaction concentration of 0.21 wt%, modification by the fluoroalkyl functionality is expected to occur with lower extents of crosslinking and multi-layer stacking. These have so-far been referred to as the fluoroalkyl modified SiO_2 (FM-SiO_2) nanoparticles.

3.2. Oil immersion resistance

The coatings embedded with FD-SiO_2 nanoparticles exhibited excellent liquid repellency performance to various low-surface tension-liquids and resistance to oil immersion. Drops of soybean oil, paraffin, cyclohexane, hexadecane and ethanol-water solutions on FD-SiO_2 coated glass slides preserved near spherical drops with high CAs of >150° and low SAs of < 10° (Fig. 3a and c).

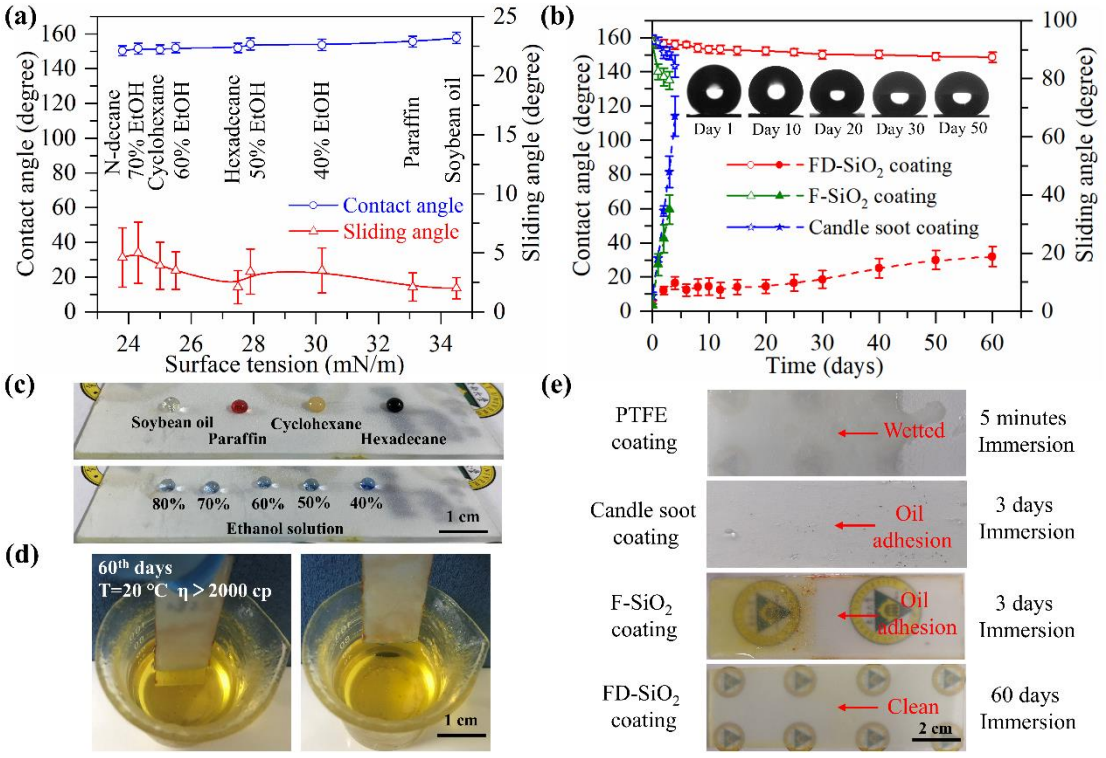

Fig. 3. Oil immersion resistance of the superamphiphobic coatings. (a) The contact angles and sliding angles of liquids with various surface tension on the coating embedded with FD-SiO_2. (b) The variation in the contact angle and sliding angle of soybean oil on different coatings after prolonged immersion in mixed oils; the inset shows drop profiles after different days of immersion of FD-SiO_2 coating. The mixed oil was composed of soybean oil and n-decane (3:1, v/v, γ = 27.4 mN/m). (c) Photographs of different low surface tension liquids and varying concentrations of ethanol-water on superamphiphobic coatings. (d) Photographs of the superamphiphobic coating embedded with FD-SiO_2 after being removed from the mixed artificial oil after 60 days of immersion at ambient temperature, without traces of oil remnants. (e) Different coatings being removed from mixed oils after 3 days of immersion. The F-SiO_2 coating was prepared based on the treatment of fluoroalkyl silane in our previous work [15]; Candle soot coating was prepared based

on the template deposition and fluoro-functionalization methods in previous literature [37]; PTFE coating was prepared via with a spray-casted commercial PTFE emulsion.

To investigate resistance to oil immersion, the superamphiphobic coating embedded with FD-SiO_2 nanoparticles was immersed in mixed artificial oils composed of soybean oil and n-decane (3:1, v/v, γ = 27.4 mN/m), simulating an actual kitchen environment. The mixed oils were evacuated in a vacuum oven to remove any dissolved gases before use. After 60 days of immersion, the coating maintained excellent oil repellency with CAs of >150° with soybean oil (Fig. 3b). Further comparative tests on state-of-the-art superamphiphobic coatings have also been benchmarked. Fig. 3b compares the results of the immersion test on a 1) superamphiphobic coating (F-SiO_2 coating) developed in our previous work [15] and 2) the superamphiphobic candle soot coating [37], respectively. Both display excellent oil repellency in the pristine state. However, under-oil immersion stability is really poor for the latter, with a rise in sliding angles beyond 30° after barely 2 days (48 hours) of immersion. Therefore, under-oil immersion stability should not be automatically attributed to the achievement of superamphiphobicity.

The appearance of coatings after being removed from the mixed oils are included in Fig. 3d and S9. After withdrawing the FM-SiO_2 coating from the mixed oils after 34 days of immersion, complete wetting films of oils were observed on surface of the FM-SiO_2 coating. In contrast, FD-SiO_2 preserved a completely clean appearance, even after 60 days of immersion at ambient temperature (Video S2), and the surface could maintain super repellency after 52 days of immersion even without the primer (Fig. S10). Optical photographs of various immersion-tested coatings are presented in Fig. 3e. After immersion for 60 days, the surface of the FD-SiO_2 coating was completely clean. On alternative coatings, and only after 3 days of immersion, many visible oil droplets were visible on the surfaces of previously developed F-SiO_2 coating [15] and the superamphiphobic candle soot coating [37]. Supplementary SEM images before and after immersion of these coatings are included in Fig. S11. With respect to a Teflon coating, a typical commercial hydrophobic coating, the mixed oils wetted the surface completely due to its comparative oleophilicity. If applied in applications requiring oil immersion, unwanted oil-fouling will occur. It is worth noting that the viscosity of the mixed oils by the end of the experiment exceeded 2000 cP, due to the natural polymerization of vegetable oils that occurs dynamically over time (Fig. S12). This dynamic increase in viscosity poses complex challenges in preventing oil penetration [38,39]. To verify stability at higher temperatures, the FD-SiO_2 coated substrate was immersed in the mixed oils and placed in an oven at 80 °C. The final viscosity reached > 1572 cp. After

50 days of immersion, the surface was withdrawn, without observable wetting or damage (Fig. S13).

So far, the FD-SiO_2 coating demonstrates fairly moderate mechanical stability, maintaining its superamphiphobicity after hand grinding (Force of 5 N, rubbing velocity of 6 cm/s) and friction tester tests (Load of 100 g) for 50 cycles, per Fig. S14. When applied for applications requiring under-oil immersion, such components are rarely mechanically contacted/abraded after installation. Thus, this level of mechanical stability is sufficient for accidental contact during initial installation and subsequent maintenance within the lifespan of the product.

3.3. Real-world tests on kitchen components

In range hoods, the impellers typically operate in air with saturated oil fumes at high rotational speeds. To evaluate oil immersion and contact resistance under harsher, accelerated dynamic conditions, the impellers with and without the

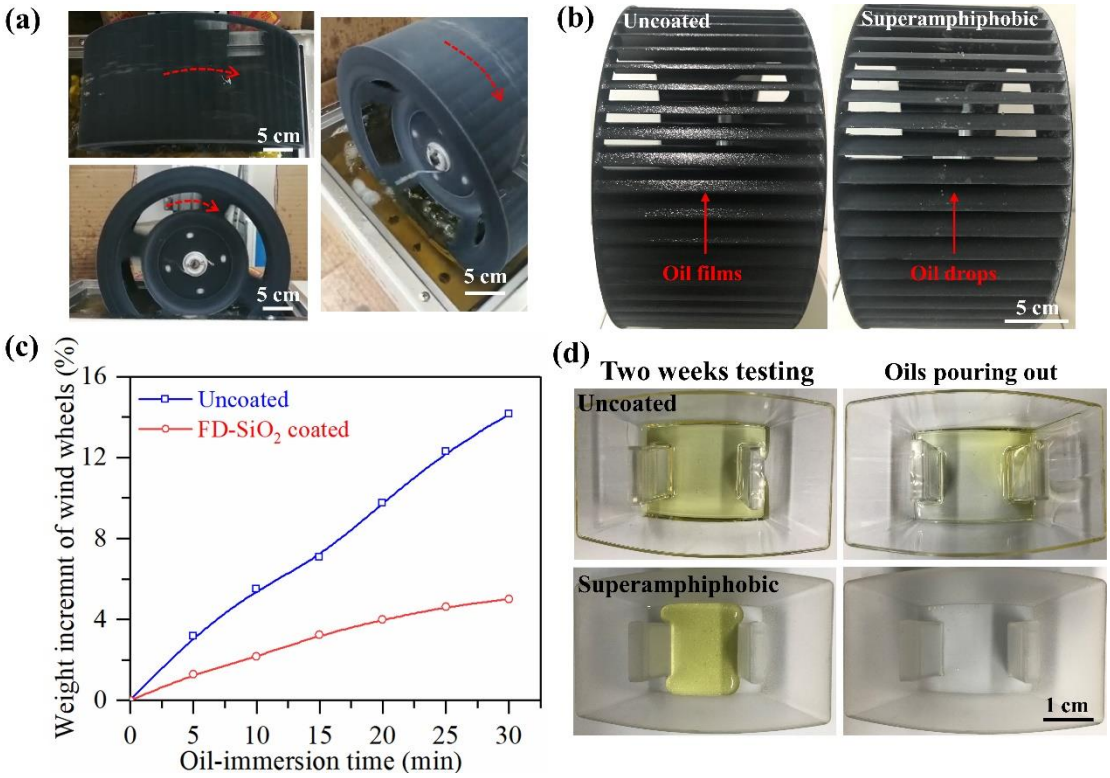

Fig. 4. The oil immersion resistance of impellers and grease traps with and without the superamphiphobic coating (FD-SiO_2). (a) Photograph of the custom-built device used in the dynamic immersion-shear test. (b) Photographs of the uncoated and superamphiphobic impellers after being removed from the oil bath. (c) The dynamic test on oil immersion of the original and superamphiphobic impellers performed in a heated oil bath (at 80 °C). (d) Photographs of the uncoated and superamphiphobic grease traps after regular kitchen operation and oil immersion for two weeks.

superamphiphobic coating composed of FD-SiO_2 were half-immersed into an oil bath and rotated at a speed of 150 r/min at 80 °C, as shown in Fig. 4a. To obtain

a quantitative analysis on this property, the increase in the weight of different impellers was presented to evaluate dynamic oil/fumes contact and immersion resistance. After performing this dynamic flow test for 120 min, as shown in Fig. 4c, the unfunctionalized impeller revealed an increase in weight of 55.6 wt%, while only 19.4 wt% was gained on the superamphiphobic impeller, suggesting almost 65% improvement on oil/fumes contact/immersion resistance of the superamphiphobic impeller. In addition, CAs and SAs of the coated and uncoated impellers have been measured to confirm the stability of the superamphiphobicity. After the dynamic rotational oil-immersion test, the superamphiphobic impeller maintained favorable oil repellency with high CAs and low SAs (Fig. S15). Alternatively, lipophilicity of original impeller has become conspicuous with oils adhering as a continuous film, showcasing much poorer oil-immersion based anti-fouling resistance. No sliding angles can be measured.

Per Fig 4b, visible oil films adhered to the surface of the original impeller after being removed from the oil bath due to the high viscosity of mixed oils. In contrast, the superamphiphobic impeller coated by FD-SiO_2 nanoparticles demonstrated much improved oil repellency (Video S3) and superior resistance to oil immersion and shear flow even under this harsher, accelerated degradation test (Video S4). Imaging of the impeller did, however, reveal a few remnant oil droplets on a few blades. Nonetheless, this still indicates considerable oil immersion resistance even under 1) accelerated testing, 2) flow shear within viscous oils and 3) heated environments. In a secondary test, grease traps with and without superamphiphobic coatings were installed in a range hood under normal cooking schedules (3 times per day for 2 hours) for assessing oil drip collection and immersion resistance within a two-week test. As depicted in Fig. 4d, it was easy to pour and remove oils from the superamphiphobic grease trap while much oily residue remained in the uncoated control.

3.4. Computation for mechanism analysis

In order to describe the improved immersion resistance of these surfaces, we evaluated the wetting pressure and impalement resistance with the use of these surfaces. We first assume a distribution of nanopores on the superamphiphobic coatings. The 3D conformation of nanoparticle-based agglomerates, radius R, can be schematized with height (H) and space (S), as shown in Fig. S16. It is known that an adequate H, coupled to a small S (high H/S ratio), the Cassie-Baxter state is achieved [40]. In this case, H must be adequate since wetting is prevented.

Under certain conditions, the Cassie state may become unstable, and liquid can penetrate the space in between particles. This impalement transition into the

so-called Wenzel state can be observed if the pressure difference between liquid and vapor phases exceeds a certain threshold value. This value is known as the impalement pressure. The impalement pressure (P_I) is the maximum pressure allowed by the geometrical constraints of the pattern before the Cassie state collapses and wetting enters the Wenzel state. Therefore, the anti-wetting pressure is represented by the impalement pressure limit (P_I, Equation (1)) generated by surface textures. We have observed high density packing of FD-SiO_2 particles (S ≈ 2R) on the optimal superamphiphobic surface from both top- and side-views (Fig. S15). From the SEM images, the mean and modal spacing is 111 ± 10 nm and 66 ± 10 nm. Owing to the dense packing, the basic Laplace pressure ($P_I = \frac{4}{\sqrt{2}}\frac{\gamma}{S}$) based impalement pressure equation no longer holds due to 1) inaccurate geometrical projection by the liquid-air interface and 2) distorted three phase contact line. A modified formula, developed by Butt. et. al., from observations of closely packed pillars, was thus implemented to describe the impalement pressure for such closely packed geometries [41].

$$P_I = \frac{2\pi\gamma R \sin\alpha \sin(\theta_a - \alpha)}{A - \pi R^2 sin^2\alpha} \quad (1)$$

$$\sin\alpha = S\sqrt{\frac{2S^2 - R^2 \sin\theta_a - 2S\cos\theta_a\sqrt{S^2 - R^2 sin^2\theta_a}}{(R^2 - 2S^2)^2 + R^2(4S^2 - R^2)\cos\theta_a}} \quad (2)$$

α is the angle describing the position of the contact line on the particle surface. θ_a is advancing contact angle (79°) of the oil on an equivalently functionalized flat surface.

In practice, oils were drip-collected into the grease trap, emulating impacting/impinging drops with velocity *V*. Therefore, the wetting pressure consists of dynamic impacting pressure [42,43] (P_D, Equation (3)), immersion-induced hydrostatic pressure (P_S, Equation (4)) and, potentially oil hammer pressure [43] (P_H, Equation (5)). Dynamic impacting pressure, P_D describes the spreading stage of impinging drops while oil hammer pressure, P_H was introduced to describe the state of initial contact. Notably, the sole balance of P_D (10 kPa) with P_I (0.81 MPa), although acceptable within an order of magnitude estimate, was however unable to describe how impalement occurred for FD-SiO_2. This limitation has been reported for the use of rigid substrates, where other contributions such as hammer pressure has been proposed [43-47]. We found that the consideration of P_H helps improve the explanations behind our observations, where surface impalement first occurs during drop impingement [43]. However, the complete formation of the partial wetting state (satellite droplets) is likely attributed to contact line pinning during drop removal [48,49].

$$P_D = \frac{1}{2}\rho V^2 \quad (3)$$

$$P_S = \rho g h \quad (4)$$

$$P_H = 0.2\rho C V \quad (5)$$

where ρ and V are the density (920 kg/m^3) and standard impinging velocity (~ 1m/s) of the oils. C is the velocity of sound in oil (~ 1324 m/s). During general usage and operation (for dripping oil drops in a kitchen environment), the P_D, P_S and P_H in this system were calculated to be ~0.46 kPa, ~0.46 kPa and ~0.24 MPa, respectively. The calculated P_I was, as described, ~0.81 MPa using the modal geometrical spacing of 66 ± 10 nm. Alternatively, the use of the mean geometrical spacing of 111 ± 10 nm results in ~0.26 MPa. Statistically, the modal spacing is more likely to experience contact during drop impingement. These limits are still greater than either P_D or P_H under use. Hence, this could explain why neither impinging oil drops nor prolonged immersion (under testing conditions) were able to induce severe penetration into the superamphiphobic surfaces.

To verify this impalement pressure limit, surfaces were impacted with oil drops from increasing heights (0.1 to 1.1 m) until impalement (Fig. S17). This resulted in increasing impinging velocity (1.41 m/s to 4.69 m/s) and correspondingly higher impact pressure. The densely packed chemical- and physical- structure of FD-SiO_2 was only penetrated at a final experimental P_D of 10 kPa and P_H of 1.14 MPa, depicted by increasing sliding angles and visible remnant satellite droplets (Fig. S13). Alternatively, FM-SiO_2 was penetrated at a much lower experimental P_H of 0.84 MPa, indicating the improved robustness of FD-SiO_2. At this junction, we emphasize the drawbacks behind using Equation (2) and (5) as quantitative proof for this system. The use of breakthrough P_H with FD-SiO_2 falls only within 29% and 77% of our theoretical estimates for P_I (modal, 66 nm) and P_I (mean, 111 nm) respectively (Fig. S13).

Despite the experimental and theoretical descriptions provided to justify the robust Cassie state of these superamphiphobic surfaces, limited depth penetration may still be inevitable. We know, from previous work, that gradual contact line motion occurs as a function of time under immersion [50]. This progression in the Z-axis (z) follows a power-law dependency on time (t).

$$\frac{dz}{dt} \alpha t^p \quad , \quad p < 0 \quad (6)$$

In their work [50], Papadopoulos et. al. concluded that alkanes with longer chain length result in a lower exponent p and slower velocity of penetration. In our system, the mixed oils are composed of soybean oil (C-18) and n-decane (C-10): the former possesses relatively long chains (C-18). This could have in part, contributed to the relatively low value of exponent p, thus giving rise to low

penetration velocity. In combination with other potential factors such as oil degradation/polymerization and viscosity increments, the penetration appears to be insignificant in influencing the functionality of the coating over extended immersion time (tested to more than an order of magnitude in time [50]).

4. Conclusions

In summary, we present a method which outlines long-term oil immersion stability using facile spray-on superamphiphobic coatings. The results are attributed to the use of densely functionalized SiO_2 nanoparticles which are densely packed in both the sub-nanoscopic (grafting density) and nanoscopic (particle-packing) scale. These coatings show superior liquid repellency for low-surface-tension liquids such as soybean oil, paraffin, cyclohexane, hexadecane, n-decane and water-ethanol mixtures, demonstrating high CAs (>150°) and low SAs (<10°). More intriguingly, they showcase superior long-term oil immersion resistance. They resisted oil infiltration even after immersion in mixed synthetic and vegetable oils for more than 50 days at both ambient (25°C) and elevated temperatures (80°C). Demonstration of scale was performed using coated ventilation impellers from range hoods, which exhibited excellent oil immersion resistance even under accelerated testing using harsh dynamic flow conditions. A marked improvement of up to 65% was achieved compared to the uncoated controls. The remarkable properties of this coating hold great promise for a wide range of potential applications such as anti-fouling surfaces for kitchenware and anti-drag surfaces for oil transportation.

Declaration of Competing Interest

There are no conflicts to declare.

Acknowledgements

The work is supported by the National Natural Science Foundation of China (Grants 52071076), the European Union's Horizon 2020 (LubISS No. 722497) for the MSCA-ESR research fellowship and the projects provided by Hisense (Guangdong) Kitchen & Bath System co., LTD and BSH Electric Appliance (Jiangsu) co., LTD.

Appendix A. Supplementary data

Supplementary data to this article can be found online at

References

[1] W. Barthlott, C. Neinhuis, Purity of the sacred lotus, or escape from contamination in biological surfaces, Planta 202 (1997) 1-8, https://doi.org/10.2307/23384993.

[2]. Z. Chu, S. Seeger, Superamphiphobic surfaces, Chem. Soc. Rev. 43 (2014) 2784-2798, https://doi.org/10.1039/c3cs60415b.

[3] D. Wang, Q. Sun, M. J. Hokkanen, C. Zhang, F. Lin, Q. Liu, S. Zhu, T. Zhou, Q. Chang, B. He, Q. Zhou, L. Chen, Z. Wang, R. H. A. Ras, X. Deng, Design of robust superhydrophobic surfaces, Nature 582 (2020) 55-59, https://doi.org/10.1038/s41586-020-2331-8.

[4] H. Liu, Y. Wang, J. Huang, Z Chen, G. Chen, Y. Lai, Bioinspired surfaces with superamphiphobic properties: concepts, synthesis, and applications, Adv. Funct. Mater. 28 (2018) 1707415, https://doi.org/10.1002/adfm.201707415.

[5] X. Wang, J. Zeng, X. Yu, Y. Zhang, Superamphiphobic coatings with polymer-wrapped particles: enhancing water harvesting, J. Mater. Chem. A 7 (2019) 5426-5433, https://doi.org/10.1039/c8ta12372a.

[6] F. Lin, S. Li, Y. Li, H. Li, L. Zhang, J. Zhai, Y. Song, B. Liu, L. Jiang, D. Zhu, Super-hydrophobic surfaces: from natural to artificial, Adv. Mater. 14 (2002) 1857-1860, https://doi.org/10.1002/adma.200290020.

[7] H. Y. Erbil, A. L. Demirel, Y. Avci, O. Mert, Transformation of a simple plastic into a superhydrophobic surface, Science 299 (2003) 1377-1380, https://doi.org/10.1126/science.1078365.

[8] W. Wang, R. Liu, H. Chi, T. Zhang, Y. Zhao, Durable superamphiphobic and photocatalytic fabrics: tackling the loss of super-non-wettability due to surface organic contamination, ACS Appl. Mater. Inter. 11 (2019) 35327-35332, https://doi.org/10.1021/acsami.9b12141.

[9] H. Liu, Y. Wang, J. Huang, Z. Chen, G. Chen, Y. Lai, Bioinspired surfaces with superamphiphobic properties: concepts, synthesis, and applications, Adv. Funct. Mater. 28 (2018) 1707415 (1-27), https://doi.org/10.1002/adfm.201707415.

[10] T. L. Liu, C. J. C. Kim, Turning a surface superrepellent even to completely wetting liquids, Science 346 (2014) 1096-1100, https://doi.org/10.1126/science.1254787.

[11] X. Li, N. Wang, J. He, Z. Yang, F. Zhao, K. Wang, C. Huang, One-step preparation of highly durable superhydrophobic carbon nanothorn arrays, Small 1907013 (2020) 1-8, https://doi.org/10.1002/smll.201907013.

[12] X. Jiao, M. Li, Z. Cheng, X. Yu, S. Yang, Y. Zhang, Recyclable superhydrophobic, antimoisture-activated carbon pellets for air and water purification, ACS Appl. Mater. Inter. 12 (2020) 25345−25352, https://dx.doi.org/10.1021/acsami.0c06274.

[13] Y. Cheng, T. Zhu, S. Li, J. Huang, J. Mao, H. Yang, S. Gao, Z. Chen, Y. Lai, A novel strategy for fabricating robust superhydrophobic fabrics by environmentally-friendly enzyme etching, Chem. Eng. J. 355 (2019) 290-298, https://doi.org/10.1016/j.cej.2018.08.113.

[14] B. N. Sahoo, N. S. K. Gunda, S. Nanda, J. A. Kozinski, S. K. Mitra, Development of dual-phobic surfaces: superamphiphobicity in air and oleophobicity underwater, ACS Sustain. Chem. Eng. 5 (2017) 6716-6726, https://doi.org/10.1021/acssuschemeng.7b00969.

[15] Z. Xiao, H. Zhu, S. Wang, W. Dai, W. Luo, X. Yu, Y. Zhang, Multifunctional superwetting composite coatings for long-term anti-icing, air purification, and oily water separation, Adv. Mater. Inter. 7 (2020) 2000013, https://doi.org/10.1002/admi.202000013.

[16] S. Pan, A. K. Kota, J. M. Mabry, A. Tuteja, Superomniphobic surfaces for effective chemical shielding, J. Am. Chem. Soc. 135 (2013) 578-581, https://dx.doi.org/10.1021/ja310517s

[17] H. Han, J. S. Lee, H. Kim, S. Shin, J. Lee, J. Kim, X. Hou, S. W. Cho, J. Seo, T. Lee, Single-droplet multiplex bioassay on a robust and stretchable extreme wetting substrate through vacuum-based droplet manipulation, ACS Nano 12 (2018) 932-941, https://doi.org/10.1021/acsnano.7b05826.

[18] L. Wu, Z. Dong, N. Li, F. Li, L. Jiang, Y. Song, Manipulating oil droplets by superamphiphobic nozzle, Small 11 (2015) 4837-4843, https://doi.org/10.1002/smll.201501021.

[19] C. T. Hsieh, F. Wu, W. Chen, Superhydrophobicity and superoleophobicity from hierarchical silica sphere stacking layers, Mater. Chem. Phys. 121 (2010) 14-21, https://doi.org/10.1016/j.matchemphys.2009.12.031.

[20] Y. Wu, M. Zhao, Z. Guo, Multifunctional superamphiphobic SiO_2 coating for crude oil transportation, Chem. Eng. J. 334 (2018) 1584-1593, https://doi.org/10.1016/j.cej.2017.11.080.

[21] J. Cheek, A. Steele, I. S. Bayer, E. Loth, Underwater saturation resistance and electrolytic functionality for superhydrophobic nanocomposites, Colloid Polym. Sci. 291 (2013) 2013-2016, https://doi.org/10.1007/s00396-013-2933-x.

[22] L. Boinovich, A. M. Emelyanenko, A. S. Pashinin, Analysis of long-term durability of superhydrophobic properties under continuous contact with water, ACS Appl. Mater. Inter. 2 (2010) 1754-1758, https://doi.org/10.1021/am100241s.

[23] W. Barthlott, T. Schimmel, S. Wiersch, K. Koch, M. Brede, M Barczewski, S. Walheim, A. Weis, A. Kaltenmaier, A. Leder, H. F. Bohn, The salvinia paradox: superhydrophobic surfaces with hydrophilic pins for air retention under water, Adv. Mater. 22 (2010) 2325-2328, https://doi.org/10.1002/adma.200904411.

[24] K. Golovin, D. H. Lee, J. M. Mabry, A. Tuteja, Transparent, flexible, superomniphobic surfaces with ultra-low contact angle hysteresis, Angew. Chem. Int. Ed. 52 (2013) 13007-13011, http://dx.doi.org/10.1002/anie.201307222.

[25] S. Pan, R. Guo, M. Björnmalm, J. J. Richardson, L. Li, C. Peng, N. Bertleff-Zieschang, W. Xu, J. Jiang, F. Caruso, Coatings super-repellent to ultralow surface

tension liquids, Nat. Mater. 17 (2018) 1040-1047, https://doi.org/10.1038/s41563-018-0178-2.

[26] S. Pan, R. Guo, J. J. Richardson, J. D. Berry, Q. A. Besford, M. Björnmalm, G. Yun, R. Wu, Z. Lin, Q. Zhong, J. Zhou, Q. Sun, J. Li, Y. Lu, Z. Dong, M. K. Banks, W. Xu, J. Jiang, L. Jiang, F. Caruso, Ricocheting droplets moving on super-repellent surfaces, Adv. Sci. 6 (2019) 1901846 (1-10), https://doi.org/10.1002/advs.201901846.

[27] W. S. Y. Wong, Surface chemistry enhancements for the tunable super-liquid repellency of low-surface-tension liquids, Nano Lett. 19 (2019) 1892-1901, https://doi.org/10.1021/acs.nanolett.8b04972.

[28] D. Zhang, G. Wu, H. Li, Y. Cui, Y. Zhang, Superamphiphobic surfaces with robust self-cleaning, abrasion resistance and anti-corrosion, Chem. Eng. J. 406 (2021) 126753, https://doi.org/10.1016/j.cej.2020.126753.

[29] T. Yeerken, W. Yu, J. Feng, Q. Xia, H. Liu, Durable superamphiphobic aramid fabrics modified by PTFE and FAS for chemical protective clothing, Prog. Org. Coat. 135 (2019) 41-50, https://doi.org/10.1016/j.porgcoat.2019.05.022.

[30] F. Wang, D. Wang, Z Guo, Highly fluorinated F-APP-TiO2 particle with hierarchical core-shell structure and its application in multifunctional superamphiphobic surface: Mechanical robustness, self-recovery and flame retardancy, J. Colloid Interface Sci. 560 (2020) 777-786, https://doi.org/10.1016/j.jcis.2019.11.014.

[31] J. Ai, Z. Guo, Biomimetic polymeric superamphiphobic surfaces: their fabrication and applications, Chem. Commun. 55 (2019) 10820-10843, https://doi.org/10.1039/c9cc03813b.

[32] Q. Li, Z. Guo, A highly fluorinated SiO_2 particle assembled, durable superhydrophobic and superoleophobic coating for both hard and soft materials, Nanoscale 11 (2019) 18338-18346, https://doi.org/10.1039/c9nr07435j.

[33] X. Li, D. Wang, Y. Tan, J. Yang, X. Deng, Designing transparent micro/nano re-entrant-coordinated superamphiphobic surfaces with ultralow solid/liquid adhesion, ACS Appl. Mater. Inter. 11 (2019) 29458-29465, https://doi.org/10.1021/acsami.9b08947.

[34] H. Wang, Z. Zhang, Z. Wang, Y. Liang, Z. Cui, J. Zhao, X. Li, L. Ren, Multistimuli-responsive microstructured superamphiphobic surfaces with large-range, reversible switchable wettability for oil, ACS Appl. Mater. Inter. 11 (2019) 28478-28486, https://doi.org/10.1021/acsami.9b07941.

[35] R. Campos, A. J. Guenthner, T. S. Haddad, J. M. Mabry, Fluoroalkyl-functionalized silica particles: synthesis, characterization, and wetting characteristics, Langmuir 27 (2011) 10206-10215, https://dx.doi.org/10.1021/la201545a.

[36] J. Yong, F. Chen, Q. Yang, J. Huo, X. Hou, Superoleophobic surfaces, Chem. Soc. Rev. 46 (2017) 4168-4217, https://doi.org/10.1039/c6cs00751a.

[37] X. Deng, L. Mammen, H.-J. Butt, Doris Vollmer, Candle soot as a template for a

transparent robust superamphiphobic coating, Science 335 (2012) 67-70, https://doi.org/10.1126/science.1207115.

[38] A. Raiyan, T. S. Mclaughlin, R. K. Annavarapu, H. Sojoudi, Effect of superamphiphobic macrotextures on dynamics of viscous liquid droplets, Sci. Rep. 8 (2018) 15344 (1-14), https://doi.org/10.1038/s41598-018-33656-9.

[39] D. Bartolo1, F. Bouamrirene1, ´E. Verneuil, A. Buguin, P. Silberzan, S. Moulinet, Bouncing or sticky droplets: impalement transitions on superhydrophobic micropatterned surfaces, Europhys. Lett. 74 (2006) 299-305, https://doi.org/10.1209/epl/i2005-10522-3.

[40] Q. Zhang, D. Sun, Y. Zhang, M. Zhu, Lattice boltzmann modeling of droplet condensation on superhydrophobic nanoarrays, Langmuir 30 (2014) 12559-12569, https://dx.doi.org/10.1021/la502641y.

[41] H. Butt, C. Semprebon, P. Papadopoulos, D. Vollmer, M. Brinkmann, M. Ciccotti, Design principles for superamphiphobic surfaces, Soft Matter 9 (2013) 418-428, https://doi.org/10.1039/c2sm27016a.

[42] D. Zang, C. Wu, R. Zhu, W. Zhang, X. Yu, Y. Zhang, Porous copper surfaces with improved superhydrophobicity under oil and their application in oil separation and capture from water, Chem. Commun. 49 (2013) 8410-8412, https://doi.org/10.1039/c3cc43536a.

[43] T. Deng, K. K. Varanasi, M. Hsu, N. Bhate, C. Keimel, J. Stein, M. Blohm, Nonwetting of impinging droplets on textured surfaces, Appl. Phys. Lett. 94 (2009) 133109 (1-3), http://dx.doi.org/10.1063/1.3110054.

[44] T. Vasileioua, J. Gerbera, J. Prautzscha, T. M. Schutziusa, D. Poulikakosa, Superhydrophobicity enhancement through substrate flexibility, Proc. Natl. Acad. Sci. USA, 113 (2016) 13307-13312, https://doi.org/10.1073/pnas.1611631113.

[45] D. Soto, H.-L. Girard, A. L. Helloco, T. Binder, D. Quéré, K. K. Varanasi1, Droplet fragmentation using a mesh, Phys. Rev. Fluids 3 (2018) 083602 (1-10), https://doi.org/10.1103/PhysRevFluids.3.083602.

[46] B. Zhao, X. Wang, K. Zhang, L. Chen, X. Deng, Impact of viscous droplets on superamphiphobic surfaces, Langmuir 33 (2017) 144-151, https://doi.org/10.1021/acs.langmuir.6b03862.

[47] H.-M. Kwon, A. T. Paxson, K. K. Varanasi, N. A. Patankar, Rapid deceleration-driven wetting transition during pendant drop deposition on superhydrophobic surfaces, Phys. Rev. Lett. 106 (2011) 036102 (1-4), https://doi.org/10.1103/PhysRevLett.106.036102.

[48] X. Deng, F. Schellenberger, P. Papadopoulos, D. Vollmer, H.-J. Butt, Liquid drops impacting superamphiphobic coatings, Langmuir 29 (2013) 7847-7856, https://dx.doi.org/10.1021/la401120j.

[49] W. S. Y. Wong, T. P. Corrales, A. Naga, P. Baumli, A. Kaltbeitzel, M. Kappl, P.

Papadopoulos, D. Vollmer, H.-J. Butt, Microdroplet contaminants: when and why superamphiphobic surfaces are not self-cleaning, ACS Nano 14 (2020) 3836-3846, https://dx.doi.org/10.1021/acsnano.9b08211.

[50] P. Papadopoulos, D. Vollmer, H. Butt, Long-term repellency of liquids by superoleophobic surfaces, Phys. Rev. Lett. 117 (2016) 046102 (1-5), https://doi.org/10.1103/PhysRevLett.117.046102.